

Ab initio exploration of short-pitch skyrmion materials: Role of orbital frustration

Takuya Nomoto^{1,*} and Ryotaro Arita^{1,2,†}

¹*Research Center for Advanced Science and Technology,
University of Tokyo, Komaba, Meguro-ku, Tokyo 153-8904, Japan*

²*RIKEN Center for Emergent Matter Science (CEMS), Wako 351-0198, Japan*
(Dated: April 4, 2024)

In recent years, the skyrmion lattice phase with a short lattice constant has attracted attention due to its high skyrmion density, making it a promising option for achieving high-density storage memory and for observing novel phenomena like the quantized topological Hall effect. Unlike conventional non-centrosymmetric systems where the Dzyaloshinsky-Moriya interaction plays a crucial role, the short pitch skyrmion phase requires a quadratic magnetic interaction $J(\mathbf{q})$ with a peak at finite- \mathbf{Q} , and weak easy-axis magnetic anisotropy is also critical. Thus, conducting first-principles evaluations is essential for understanding the formation mechanism as well as for promoting the discovery of new skyrmion materials. In this *Perspective*, we focus on recent developments of the first-principles evaluations of these properties and apply them to the prototype systems $\text{Gd}T_2X_2$ and $\text{Eu}T_2X_2$, where T denotes a transition metal and X represents Si or Ge. In particular, based on the spin density functional theory with the Hubbard correction combined with the Liechtenstein method in the Wannier tight-binding model formalism, we first show that the Hubbard U and Hund's coupling is essential to stabilize a skyrmion lattice state by enhancing the easy-axis anisotropy. We then discuss mechanisms of finite- \mathbf{Q} instability and show that competition among Gd-5d orbitals determines whether ferromagnetism or a finite- \mathbf{Q} structure is favored in $\text{Gd}T_2\text{Si}_2$ with $T = \text{Fe}$ and Ru . Our systematic calculations reveal that GdRu_2X_2 , GdOs_2X_2 , and GdRe_2X_2 are promising, while GdAg_2X_2 , GdAu_2X_2 , and EuAg_2X_2 are possible candidates as the skyrmion host materials. Analysis based on a spin spiral calculation for the candidate materials is also presented.

I. INTRODUCTION

A magnetic skyrmion is a particle-like topological spin texture realized in condensed matter systems. Its magnetization distribution is characterized by vorticity, helicity, and a winding number, and the coupling to an itinerant electron provides a unique platform for exploring the physics under the emergent gauge field [1–3]. The skyrmion is also considered a candidate element in future magnetoelectric devices due to its stability against an external perturbation and high controllability by an electric current [4–8]. Particularly, a racetrack memory [9], a magnetic random access memory [10, 11], and an artificial synapse for neuromorphic computing [12, 13] are promising applications of the topologically stable magnetic object.

The magnetic skyrmions form a two-dimensional lattice in a ferromagnetic background. While an array of magnetic bubbles or skyrmions has been observed in a magnetic thin film since the 1970s [14, 15], the first observation in a bulk magnet was accomplished in 2009 by the neutron scattering measurement for MnSi with B20 crystal structure [16]. In the chiral magnet, an early theory suggested that a Dzyaloshinsky-Moriya (DM) interaction is the key to realizing the skyrmion lattice phase [17, 18]. Namely, the competition between ferromagnetic and DM interaction induces a non-collinear spin spiral structure, whose modulation pitch is determined by A/D with A be-

ing magnetic stiffness and D being a DM constant. Once the spiral state is stabilized, a triple- \mathbf{Q} state, which is identical to the triangular skyrmion lattice, is expected to appear under a magnetic field due to the momentum conservation of the quartic term in the Ginzburg-Landau functional. Today, there are many materials showing the DM-induced skyrmion phase in bulk, thin film, and heterostructures. In these systems, a typical modulation pitch is around 10-100nm, much larger than the lattice constant since $D \ll A$ is satisfied in most cases [19–23].

On the other hand, the magnetic skyrmion observed in the centrosymmetric crystals has recently attracted much attention, where the DM interaction should not play any role. The first observation was reported in Gd_2PdSi_3 with Gd forming a two-dimensional triangular lattice network [24, 25], followed by $\text{Gd}_3\text{Ru}_4\text{Al}_{12}$ with a Kagome lattice [26], GdRu_2Si_2 [27], EuAl_4 [28–31], and EuGa_4 [30, 32] with a square lattice network. A remarkable feature of the skyrmion lattice in centrosymmetric systems is its relatively shorter modulation pitch, typically given by a few nanometers. Since this does not originate from the DM interaction, its formation mechanism has been intensively studied recently. In terms of the shortness of the modulation pitch, the skyrmion lattices observed in EuPtSi [33, 34] and $\text{Mn}_{1-x}\text{Fe}_x\text{Ge}$ [35, 36] might be classified into the same category as the centrosymmetric systems even though their crystal structures do not have the space inversion symmetry. Since a short-pitch skyrmion lattice is favorable for realizing high-density memory bits in a storage device, revealing the key quantity to determine the modulation pitch will promote further materials design and engineering of the

* nomoto@ap.t.u-tokyo.ac.jp

† arita@riken.jp

skyrmion phase. Furthermore, the high skyrmion density of the short-pitch skyrmion is of great theoretical importance, as it provides a unique platform to observe fascinating phenomena, such as a quantized topological Hall effect [37] and a crossover behavior of the topological Hall effect where both the real-space and momentum-space Berry curvature play a crucial role [38].

To date, there have been a lot of theoretical works on the formation of a short-pitch skyrmion lattice. They include calculations based on a classical spin model, an itinerant electron model, and an effective Ginzburg-Landau functional. These theories enable us to grasp a physical insight into the skyrmion lattice formation and, indeed, the importance of the magnetic frustrations [39, 40], compass anisotropy of the magnetic interactions [41, 42], higher-order spin interactions [43, 44], and Fermi surface nesting [45, 46] have been recognized as an essential property to stabilize the skyrmion lattice phase (for more details, see Ref. [47]). However, these model calculations are usually performed with a given modulation vector and include adjustable parameters. Thus, they have no predictive power for the modulation pitch itself in real materials. On the other hand, in spite of the expensive numerical cost, one can investigate the stability of finite- Q spin spiral structures from first-principles, which is helpful to see the origin of the modulation pitch and its material dependence. Indeed, the calculations for GdRu₂Si₂ [48, 49], Gd₂PdSi₃ [48, 49], and MnGe [50, 51] have successfully unveiled microscopic mechanisms in stabilizing their short-pitch skyrmion phase. Thus, broadening the target compounds along this line is of great importance, helping us understand the material dependence more deeply and promoting the discovery of new skyrmion materials.

Based on the theory for short-pitch skyrmion phase, a promising system for observing skyrmion phases should possess weak easy-axis anisotropy and spin-spin interactions favoring finite- Q modulations [47]. Since these effects on skyrmion formation are well-established, in this *Perspective*, we aim to highlight recent progress in first-principles evaluations of these properties and offer predictive insights to guide experimental efforts in discovering new skyrmion materials. To achieve this, based on spin density functional theory (SDFT) and SDFT with the Hubbard correction U (SDFT+ U), we perform systematic first-principles calculations for GdT₂X₂ and EuT₂X₂ with T being a transition metal element and X being Si or Ge. Since the largest number of skyrmion compounds have been found in this ThCr₂Si₂-type crystal structure, these compounds would be ideal target materials. First, we show that the inclusion of U and Hund's coupling J is essential to obtain easy-axis anisotropy, which is necessary for stabilizing a skyrmion lattice than a spin spiral state. Then, we evaluate magnetic interactions $J(\mathbf{q})$ based on the so-called Liechtenstein method with the Wannier tight-binding model formalism. The calculated $J(\mathbf{q})$ is in good agreement with $E(\mathbf{q})$ directly evaluated by the spin spiral calculations within SDFT+ U , support-

ing the validity of the present Liechtenstein calculations. Based on the results, we argue that the finite- Q structure is determined not only by the shape of the Fermi surface but also by the details of the electronic structure. Especially, we show that competition among the Gd-5d orbital contributions determines whether a ferromagnetism or finite- Q structure is favored in GdT₂Si₂ with $T = \text{Fe}$ and Ru . According to our systematic calculations, GdRu₂X₂, GdOs₂X₂, GdW₂X₂, GdRe₂X₂, GdAg₂X₂, GdAu₂X₂, EuCo₂X₂, and EuAg₂X₂ with $X = \text{Si}$ and Ge are possible candidates for showing the skyrmion phase. The present study provides a firm ground to discover and design the short-pitch skyrmion phase from systematic calculations, and the extension to the other crystal structures will be a promising future development.

II. METHODS

In this section, we summarize the methods used in this *Perspective*. First, we explain the evaluation of $J(\mathbf{q})$ based on the Liechtenstein method. Although this method was first formulated in the multiple scattering theory with the Green's function techniques, it has been applied to the SDFT Hamiltonian with various spatially localized bases, including the Wannier functions [52, 53]. Here, we show the formulation following Ref. [53]. We begin with the following tight-binding Hamiltonian,

$$H = \sum_{12} (t_{12} + v_{12}) c_1^\dagger c_2, \quad (1)$$

where indices 1 and 2 run over all degrees of freedom that specify the Wannier functions, including atomic sites i , orbitals ℓ , and spins σ . c_1^\dagger (c_1) represents an electron creation (annihilation) operator in this basis. t_{12} and v_{12} denote spin-independent and spin-dependent hopping integral matrices, respectively. These parameters are extracted from the SDFT/SDFT+ U calculation with ferromagnetic reference states through the Wannier construction process [54, 55].

Based on the Hamiltonian (1), we can evaluate the magnetic interaction J_{ij} in the classical Heisenberg model as follows,

$$J_{ij} = -\frac{1}{2} \text{Tr}_{n\ell\sigma} [G_{ij}(\omega_n) \Sigma^i G_{ji}(i\omega_n) \Sigma^j]. \quad (2)$$

Here, $\text{Tr}_{n\ell\sigma} = T \sum_n \text{Tr}_{\ell\sigma}$, where $\text{Tr}_{\ell\sigma}$ denotes the trace over the orbital and spin spaces. $\omega_n = \pi T(2n+1)$ denotes the Matsubara frequency, and T is the temperature. The Green's function $G(\omega_n)$ and the magnetic perturbation matrix at i site Σ^i are defined by,

$$[G(\omega_n)]_{12}^{-1} = i\omega_n \delta_{12} - t_{12} - v_{12} \quad (3)$$

$$\Sigma_{12}^i = \tilde{v}_{i\ell_1, i\ell_2} \sigma_{\sigma_1\sigma_2}^x \quad (4)$$

where we approximate Σ_{12}^i as a local quantity. σ^μ ($\mu = x, y, z$) is the Pauli matrix, and $\tilde{v}_{i\ell_1, i\ell_2}$ is defined by $v_{i\ell_1\sigma_1, i\ell_2\sigma_2} = \tilde{v}_{i\ell_1, i\ell_2} \sigma_{\sigma_1\sigma_2}^z$. Then, $G_{ij}(\omega_n)$

is defined as a sub-matrix of $G_{12}(\omega_n)$ having (i, j) sites component. The evaluation of the Matsubara summation in Eq. (2) is performed by the sparse sampling technique with the intermediate representation [56, 57]. More details about the implementation are found in Ref. [53]. Based on J_{ij} evaluated by Eq. (2), its Fourier transform $J(\mathbf{q})$ is obtained as follows:

$$J(\mathbf{q}) = \frac{1}{N} \sum_{ij} e^{-i\mathbf{q}\cdot(\mathbf{R}_i - \mathbf{R}_j)} J_{ij} - J_0, \quad (5)$$

where \mathbf{R}_i denotes the real space coordinate of the site i including the relative coordinate of the sublattice. Here, we have introduced J_0 , the on-site magnetic interaction, to guarantee the absence of the self-interaction term in the Heisenberg model. Note that, although J_{ij} evaluated by Eq. (2) will be finite for non-magnetic sites such as a transition metal T and $X = \text{Si, Ge}$ in GdT_2X_2 and EuT_2X_2 , the i, j summation in Eq. (5) should be taken only for the magnetic site, namely, Gd or Eu site in our cases. Indeed, J_{ij} connecting non-magnetic elements can take a large value when both the density of states (DOS) and exchange splitting near the Fermi level are finite, although the mapping into the classical spin model for these orbitals is totally inadequate. This procedure can remove this artificial contribution in the evaluation of $J(\mathbf{q})$, which is essential for the SDFT+ U calculations. Based on the obtained $J(\mathbf{q})$, we can see whether the system favors the finite- \mathbf{Q} modulation.

On the other hand, we can evaluate the energy of the spin spiral states with the modulation vector \mathbf{Q} , denoted by $E(\mathbf{q})$, within SDFT and SDFT+ U . The calculation is based on the generalized Bloch theorem, in which the energy of the spin spiral state is evaluated with specific twisted boundary conditions for the Bloch spinors [58]. A clear advantage of this method is that the calculated $E(\mathbf{q})$ is exact within the SDFT/SDFT+ U level, and no assumption of the mapping to the classical spin model is introduced. Moreover, it is not necessary to expand the unit cell even when calculating the finite- \mathbf{Q} structure, which makes the calculation with small \mathbf{Q} tractable. However, despite these advantages, it requires a calculation for every \mathbf{Q} , and thus, is much more expensive than the Liechtenstein method if one wants to see the detailed structures of $E(\mathbf{q})$. Thus, we use these two methods in a complementary manner.

III. CALCULATION DETAILS

For the evaluations of $J(\mathbf{q})$ and $E(\mathbf{q})$, we use Vienna *ab initio* simulation package (VASP) [59] for the electronic structure calculations. Here, the exchange-correlation functional proposed by Perdew, Burke, and Ernzerhof [60], and pseudopotentials with the projector augmented wave (PAW) basis [61, 62] are used. The spin orbit interaction is neglected except for the magnetocrystalline anisotropy calculations.

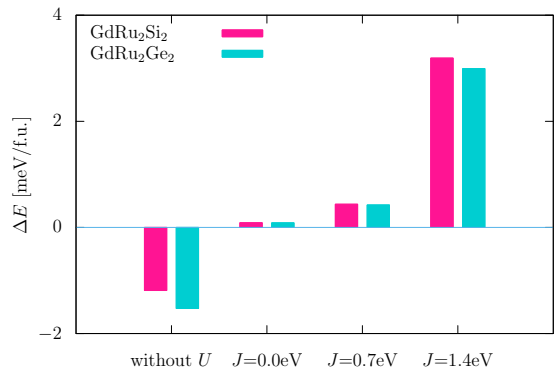


FIG. 1. Magnetocrystalline anisotropy of GdRu_2Si_2 and GdRu_2Ge_2 . The label “without U ” stands for the result of the standard SDFT calculation. The others correspond to SDFT+ U calculations with $U = 6.7$ eV.

The structure optimization is performed for all GdT_2X_2 and EuT_2X_2 compounds by the SDFT+ U method assuming ferromagnetic states. The convergence criteria of the structure optimization is set to 10^{-5} eV and the corresponding electronic self-consistent loop is 10^{-6} eV with the accurate precision mode. Here, we use a $16 \times 16 \times 16$ Monkhorst-Pack \mathbf{k} -mesh, and a cutoff of the plane wave basis set is set to be twice the recommended maximum value of the cutoff. For the magnetocrystalline anisotropy calculations, we employ 10^{-8} eV as the convergence criteria for electronic calculations and $21 \times 21 \times 21$ Monkhorst-Pack \mathbf{k} -mesh. The cutoff is set to be twice the recommended value. For the energy calculations of the spin spiral states, we employ 10^{-8} eV as the convergence criteria for electronic calculations, $16 \times 16 \times 16$ Monkhorst-Pack \mathbf{k} -mesh, and the cutoff is 2.5 times as large as the recommended values.

For constructing the Wannier tight-binding model, we use 156 Bloch states evaluated on $10 \times 10 \times 10$ uniform \mathbf{k} -grid in the disentanglement procedure. The trial orbitals are set to the Gd/Eu- d and f orbitals, transition metal T - s , p , and d orbitals, and $X = \text{Si/Ge}$ - s and p orbitals. The outer window is set as it includes all 156 Bloch states, and the inner window is set as it covers from the bottom of the bands to the bands at 4 eV above the Fermi level. The obtained tight-binding model consists of 38 orbitals per spin. Based on the obtained tight-binding model, J_{ij} and $J(\mathbf{q})$ are evaluated by Eqs. (2) and (5), respectively. Here, we set the temperature $T = 58$ K and employ 48×48 uniform \mathbf{k} -grid.

IV. RESULTS AND DISCUSSION

A. Magnetocrystalline anisotropy

According to the theory of skyrmion lattice formation [47], the system should possess two properties to realize a skyrmion lattice phase in a broad region of parameter space. Namely, it is necessary that the spin in-

teraction is compatible with a finite- Q modulation, and the magnetocrystalline anisotropy is the easy axis type as well as sufficiently weak. It should be noted that, with the exception of Gd^{3+} and Eu^{2+} , rare earth elements possess a finite orbital moment with strong spin-orbit coupling, leading to strong magnetocrystalline anisotropy in most cases. As a result, compounds containing these elements are unlikely to exhibit the weak magnetocrystalline anisotropy required for the formation of skyrmion lattice phases. Therefore, in this *Perspective*, we only consider Gd^{3+} - and Eu^{2+} -based compounds, where the orbital angular momentum of their $4f$ -orbitals are almost quenched in the ionic ground states. On the other hand, there is no general trend for these elements, whether the anisotropy is the easy axis or easy plane type. Thus, it is crucial to see whether the system shows the correct magnetic anisotropy before discussing the modulation vectors based on the electronic structure.

As an example, let us first see in Fig. 1 the calculated magnetocrystalline anisotropy,

$$\Delta E := E(\mathbf{m}/\mathbf{x}) - E(\mathbf{m}/\mathbf{z}) \quad (6)$$

for the skyrmion compound GdRu_2Si_2 and a reference compound GdRu_2Ge_2 [63]. We can see that the energy scale of the magnetic anisotropy is quite small, $|\Delta E| < 5$ meV per formula unit, as expected. However, the sign of ΔE is negative in the SDFT results, indicating that a helical magnetic structure is expected to have a lower energy than the skyrmion state. This situation drastically changes by including the Hubbard correction U . In the case of Gd^{3+} , since U enhances the energy difference between the lowest energy state with $L = 0$ and the first excited state with $L \neq 0$, we can expect that the magnetocrystalline anisotropy decreases by increasing the value of U , which is consistent with the results in Fig. 1. Notably, ΔE becomes small but positive with $U = 6.7$ eV even without Hund's coupling correction J . In addition, we can also see that the anisotropy becomes larger positive with increasing the strength of J , which is compatible with the observed skyrmion lattice phases. This result clearly indicates that the inclusion of U and J is essential to obtain the correct magnetocrystalline anisotropy in the Gd and Eu-based skyrmion materials.

Figures 2(a-d) summarize the results of ΔE in all Gd and Eu-based 122 compounds that we discuss for this *Perspective*. We can see that, for most transition metal T except for Ta, the SDFT+ U results show the same or lower $|\Delta E|$ than SDFT, which is similar to the cases of GdRu_2Si_2 and GdRu_2Ge_2 . Although the values of ΔE highly depend on the host f -element and Eu-based compounds tend to have considerable negative ΔE in SDFT, these trends are strongly suppressed in SDFT+ U . In SDFT+ U , ΔE is no longer sensitive to the transition metal T and the group 14 element $X = \text{Si}$ and Ge . Also, the amplitude $|\Delta E|$ is sufficiently small and $|\Delta E| < 3$ meV/f.u. is satisfied in all compounds. It is worth noting that only one (seven) in GdT_2X_2 (EuT_2X_2) among all 48 compounds considered show negative ΔE , implying that

the weak easy-axis anisotropy is an intrinsic property inherent in this ThCr_2Si_2 -type crystal structure.

B. Fermi surface and magnetic instability

Next, let us move on to the modulation vector of GdT_2X_2 and EuT_2X_2 . According to the previous discussion, it is essential to include the local Coulomb repulsion U and Hund's coupling J to reproduce the correct magnetocrystalline anisotropy observed in the experiments. Thus, in the present study, we discuss the modulation vector \mathbf{Q} based on the electronic structures in the SDFT+ U calculations. Apparently, the effect of U and J on \mathbf{Q} should not be significant if \mathbf{Q} is determined only by the shape of the Fermi surface, which is often supposed in the RKKY scenario for the skyrmion lattice formation. Indeed, since the magnetic moments of Gd^{3+} and Eu^{2+} are fully polarized even in the absence of U and J , the Fermi surface is expected to be insensitive to the values of U and J . We can directly confirm that magnetic moments are fully polarized in the ferromagnetic states in most compounds except for EuMn_2Si_2 , EuZr_2Si_2 , EuZr_2Ge_2 , EuTc_2Si_2 , EuTc_2Ge_2 , EuHf_2Ge_2 , EuTa_2Si_2 and EuRe_2Ge_2 . Thus, although the electronic structure above the Fermi energy should be modified to some extent because of the change of the exchange splitting, this will not affect the modulation vector \mathbf{Q} in the skyrmion phase.

The insensitivity of the Fermi surface against U and J can be seen directly by the band structure calculations. For example, we show the band structures near the Fermi levels of GdRu_2Si_2 and GdFe_2Si_2 in Figs. 3(a-d). Here, the majority and minority bands calculated with SDFT and SDFT+ U are plotted, respectively. We can see from the figures that, although they differ in detail especially above the Fermi levels, U and J do not change the Fermi surface, which means that SDFT and SDFT+ U results share the same Fermi surface instability. Note that this trend is valid for all compounds when SDFT correctly captures the ionic state of Gd^{3+} and Eu^{2+} .

In the continuum model, it is well-known that the Lindhard function describes the Fermi surface instability. In a real material with many bands, the nesting function,

$$\chi_{nn'}(\mathbf{q}) = -\frac{1}{N} \sum_{\mathbf{k}} \frac{f(\varepsilon_{n\mathbf{k}+\mathbf{q}}) - f(\varepsilon_{n'\mathbf{k}})}{\varepsilon_{n\mathbf{k}+\mathbf{q}} - \varepsilon_{n'\mathbf{k}}}, \quad (7)$$

plays the same role. Here, n and \mathbf{k} denote the band index and crystal momentum, respectively. $\varepsilon_{n\mathbf{k}}$ is the eigenvalues of the Bloch states having n and \mathbf{k} , and $f(\varepsilon)$ is the Fermi distribution function. The nesting function is sometimes considered to describe not only the Fermi surface instability but also the spin instability, such as spin-density-wave and helical \mathbf{Q} magnetic structures. However, as is known in the fluctuation theory for multi-orbital systems, the orbital character of the bands is essential to describe the fluctuation. In this case, it is

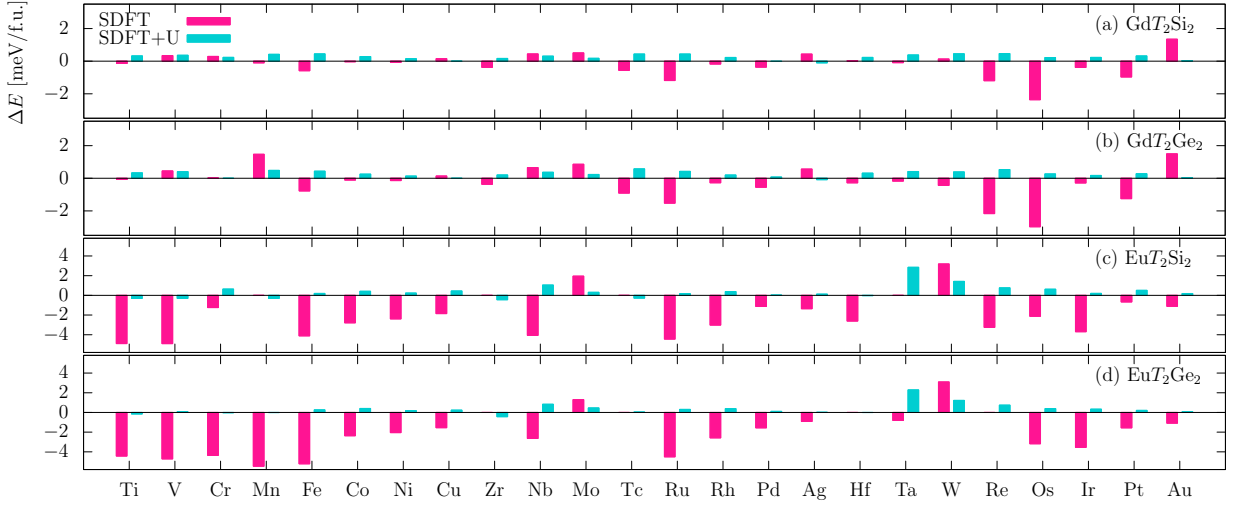


FIG. 2. Magnetocrystalline anisotropy of (a) GdT_2Si_2 , (b) GdT_2Ge_2 , (c) EuT_2Si_2 and (d) EuT_2Ge_2 . The SDFT+ U results stand for the calculations with $U = 6.7$ eV and $J = 0.7$ eV. Note that the data for EuMn_2Si_2 , EuZr_2Si_2 , EuZr_2Ge_2 , EuTc_2Si_2 , EuTc_2Ge_2 , EuHf_2Ge_2 , EuTa_2Si_2 and EuRe_2Ge_2 in SDFT, and GdCr_2Ge_2 in SDFT+ U are not shown. This is because the fully polarized ferromagnetic solutions along the x and/or z axis are unstable for these materials.

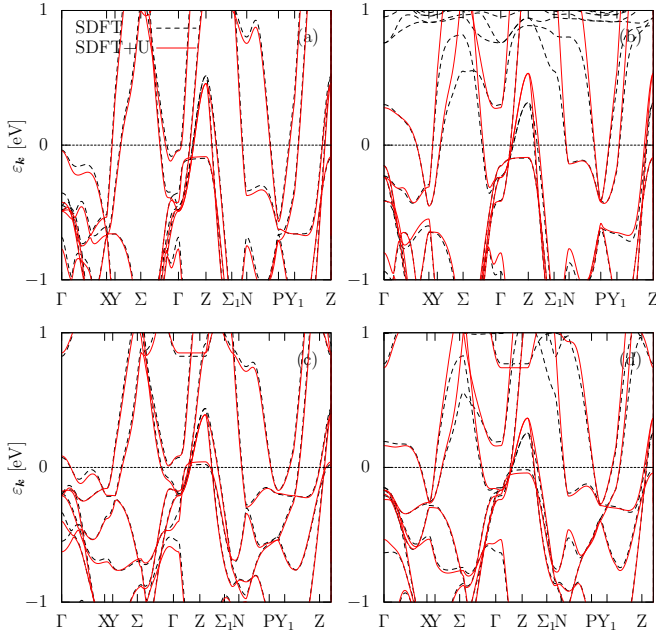


FIG. 3. Band structures of (a) majority spin of GdRu_2Si_2 , (b) minority spin of GdRu_2Si_2 , (c) majority spin of GdFe_2Si_2 and (d) minority spin of GdFe_2Si_2 . Solid lines correspond to SDFT and dashed lines correspond to SDFT+ U results with $U = 6.7$ eV and $J = 0.7$ eV.

necessary to consider the (zeroth-order) spin correlation function $\chi_{\mu\nu}(\mathbf{q})$ defined as follows,

$$\chi_{\mu\nu}(\mathbf{q}) = \frac{1}{N} \sum_{\mathbf{R}} \sum_{1234} e^{i\phi_{13}^{\mathbf{q}}(\mathbf{R})} s_{13}^{\mu} s_{24}^{\nu} \chi_{13,24}(\mathbf{R}), \quad (8)$$

$$\chi_{13,24}(\mathbf{R}) = -T \sum_{\omega_n} G_{12}(i\omega_n, \mathbf{R}) G_{43}(i\omega_n, -\mathbf{R}). \quad (9)$$

Here, the phase $\phi_{12}^{\mathbf{q}}(\mathbf{R})$ is defined by $\phi_{12}^{\mathbf{q}}(\mathbf{R}) = \mathbf{q} \cdot (\mathbf{R}_{i_1} - \mathbf{R}_{i_2})$, and ω_n and ω_q denote the Fermionic and Bosonic Matsubara frequency, respectively. Since Eq. (9) leads to the nesting function with a modification due to the transformation from local orbital to band basis, the \mathbf{q} -dependence of $\chi_{\mu\nu}(\mathbf{q})$ is mainly determined by Eq. (7). However, it should be noted that the basis transformation gives an additional source of the \mathbf{q} -dependence, and $\chi_{\mu\nu}(\mathbf{q})$ is sensitive not only to the shape of the Fermi surface but also to its orbital character. Moreover, in the strongly correlated electron systems, Eqs. (8) and (9) are not sufficient to describe the correct spin fluctuation. In this case, the effect of U must be taken more accurately using a diagrammatic technique, which is practically impossible in most cases. In that sense, the Liechtenstein method presented provides a simple but reliable approximation in taking the correlation effects. Indeed, it is known that this method successfully reproduces the result of t/U expansion in the strong correlation limit and reproduces Eqs. (8) and (9) in the weak correlation limit. It is worth noting that in the intermediate and strong U regime, not only the Fermi surface but also the electronic structure far from the Fermi level can affect the spin instability.

C. $J(\mathbf{q})$ in GdRu_2Si_2 and GdFe_2Si_2 evaluated by the Liechtenstein method

Figures 4(a) and (b) show $J(\mathbf{q})$ for GdRu_2Si_2 and GdFe_2Si_2 calculated based on the Liechtenstein formula, Eq. (5). The result in Fig. 4(a) shows good agreement with that in Ref. [49] but is slightly different from that in Ref. [48] due to an erroneous treatment of the phase factor in Eq. (8). According to the results, since the peak

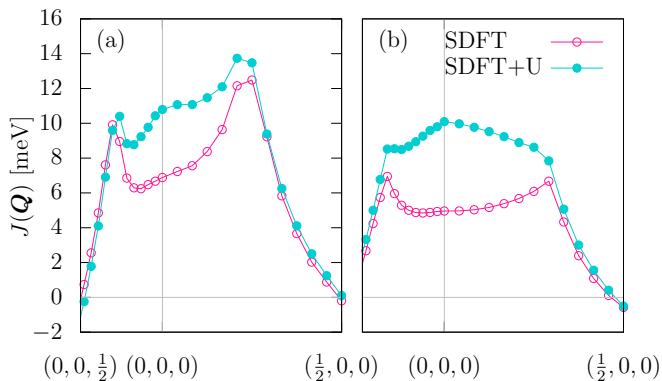


FIG. 4. Modulation vector \mathbf{Q} dependence of the spin exchange interaction $J(\mathbf{q})$ in (a) GdRu_2Si_2 and (b) GdFe_2Si_2 calculated based on the Liechtenstein formula. A pink (cyan) line with open (filled) circle corresponds to the SDFT (SDFT+ U with $U = 6.7$ eV and $J = 0.7$ eV) result.

position \mathbf{Q} in $J(\mathbf{q})$ is the signature of magnetic instability with the modulation vector \mathbf{Q} , we can say that GdRu_2Si_2 favors the spin spiral state with $\mathbf{Q} \sim (0.25, 0, 0)$ both in SDFT and SDFT+ U . On the other hand, in GdFe_2Si_2 , finite- \mathbf{Q} instability is seen only in SDFT while SDFT and SDFT+ U give the same Fermi surface (see Figs. 3(c) and (d)). This result indicates that the finite- \mathbf{Q} structure is determined not only by the shape of the Fermi surface but also by other factors, such as an orbital character and electronic structure far from the Fermi level.

The ferromagnetic instability observed in the SDFT+ U calculation for GdFe_2Si_2 is also found in the spin spiral calculation (which will be discussed in Section IV F). However, it seems to be inconsistent with the observed spin flop transition in GdFe_2Si_2 [64], which implies that we may need to treat the correlation effect more precisely to understand the magnetism in GdFe_2Si_2 . On the other hand, GdRu_2Si_2 has a peak at $\mathbf{Q} \sim (0.25, 0, 0)$ both in SDFT+ U and SDFT calculation, similar to the previous results based on SDFT (without U) [48, 49], which is consistent with the experiment.

Note that, in principle, it is necessary to perform a spin model simulation to find out a correct magnetic ground state, especially for multiple- \mathbf{Q} states like a skyrmion lattice phase. For a spin model of GdRu_2Si_2 , an analysis based on the Landau-Lifshitz-Gilbert (LLG) equation was performed in Ref. [49], using the following model for the internal energy,

$$E = -\frac{1}{2} \sum_{ij} J_{ij} \mathbf{m}_i \cdot \mathbf{m}_j - K \sum_i (\mathbf{m}_i \cdot \mathbf{e}_z)^2 - \mathbf{B} \cdot \sum_i \mathbf{m}_i, \quad (10)$$

where K is a magnetocrystalline anisotropy constant, and \mathbf{B} is a external magnetic field applied along the c axis. They solved the LLG equations for Eq. (10) with J_{ij} evaluated from first-principles, which is consistent with Fig. 4(a), and obtained a magnetic phase diagram in terms of K and B , as shown in Fig. 5. According to

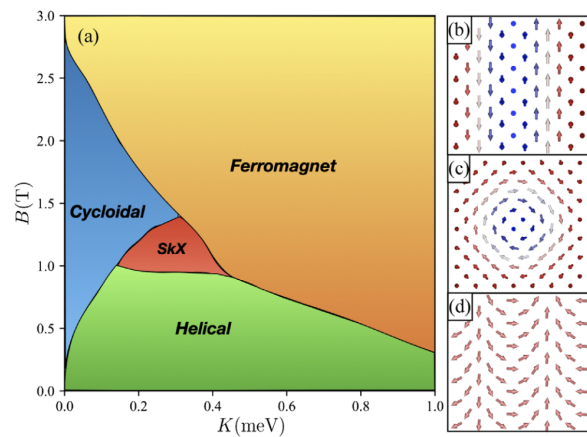


FIG. 5. (a) A magnetic phase diagram of GdRu_2Si_2 in the (K, B) parameter space, where K is the magnetocrystalline anisotropy and B is the magnetic field. (b)-(d) Representative magnetic textures described by the Gd moments. (b) Helical state for $(K, B) = (0.2, 0.6)$, (c) Skyrmion state for $(K, B) = (0.2, 1.0)$, and (d) cycloidal state for $(K, B) = (0.1, 1.0)$. Reproduced from Ref. [49].

Fig. 5, the skyrmion lattice phase appears when the easy-axis anisotropy K is in the range from 0.2 to 0.4 meV. On the other hand, as discussed in the previous sections, the SDFT+ U calculation reproduces the easy-axis anisotropy of GdRu_2Si_2 . The value of K in GdRu_2Si_2 is ~ 0.43 meV, which is in good agreement with the spin model simulation. Note that the significance of weak easy-axis anisotropy can be straightforwardly understood: if the anisotropy is easy-plane type, a helical single- \mathbf{Q} state is favored over multiple- \mathbf{Q} states like a skyrmion phase, and if the easy-axis anisotropy is too strong, Ising-type magnetic order is favored over finite- \mathbf{Q} structures. Thus, we conclude that the SDFT+ U result in GdRu_2Si_2 is fully consistent with the observation of the skyrmion lattice phase, and the present method correctly captures the essential physics behind the magnetic structure.

D. Orbital decomposition of $J(\mathbf{q})$ calculated based on the Liechtenstein method

One of the advantages of evaluating $J(\mathbf{q})$ based on the tight-binding formalism is that it is easy to discuss the microscopic origin of the magnetic interaction [48, 65]. Although $J(\mathbf{q})$ was decomposed into the Gd-4*f* and 5*d* components and a possible frustration mechanism between these two was discussed in Ref. [48], one may think that the situation will be different in a real material since their calculations were based on the SDFT electronic structures. Indeed, with the SDFT+ U results, we can easily show that the contribution from Gd-4*f* orbital is strongly suppressed and never affect the modulation vector of the helical states, as shown in Fig. 6(a). Naively, this indicates the absence of conventional RKKY interac-

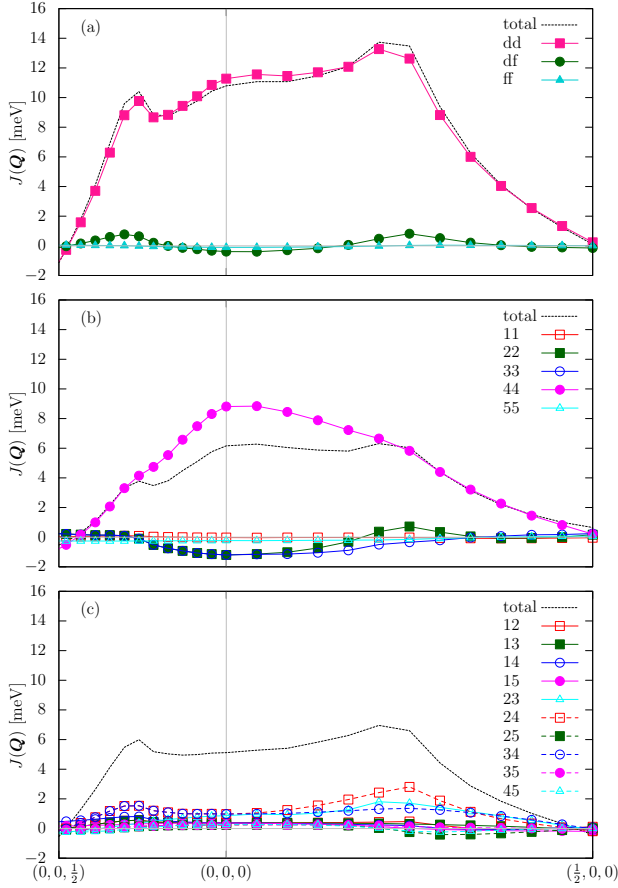


FIG. 6. Orbital decomposed $J(\mathbf{q})$ calculated by the Liechtenstein method. (a) The contributions from the Gd-5d and 4f orbitals. (b) The diagonal contribution to in the Gd-5d manifold. Here, the indices 1 to 5 correspond to the d_{z^2} , d_{xz} , d_{yz} , $d_{x^2-y^2}$, and d_{xy} orbitals, respectively. (c) The off-diagonal contributions in the Gd-5d manifold.

tions in this compound since it is included in the Gd-4f contribution as discussed in Ref. [48]. On the other hand, as seen in the previous subsections, the orbital character and the electronic structures not at the Fermi level are essential factors in determining the finite- \mathbf{Q} instability. Since the \mathbf{q} dependence of $J(\mathbf{q})$ mainly comes from the Gd-5d manifold according to Fig. 6(a), it would be interesting to decompose $J(\mathbf{q})$ into each 5d orbital based on the SDFT+ U electronic structures.

Figure 6(b) and (c) show the diagonal and off-diagonal contributions to $J(\mathbf{q})$ in the Gd-5d manifold, respectively. Among the five 5d orbitals, the contributions from the d_{z^2} and d_{xy} orbitals are negligibly small, and the \mathbf{q} dependence of $J(\mathbf{q})$ originates from the remaining three orbitals. Among the three, we can see that only the diagonal contribution from the $d_{x^2-y^2}$ orbital has a peak structure at the Γ point, favoring the ferromagnetic ground state. In contrast, the other diagonal and off-diagonal ones show the peak at $\mathbf{Q} \sim (0.25, 0, 0)$ or almost flat along the Γ -X line. These results indicate that the orbital frustration exists in the 5d orbital manifold, and

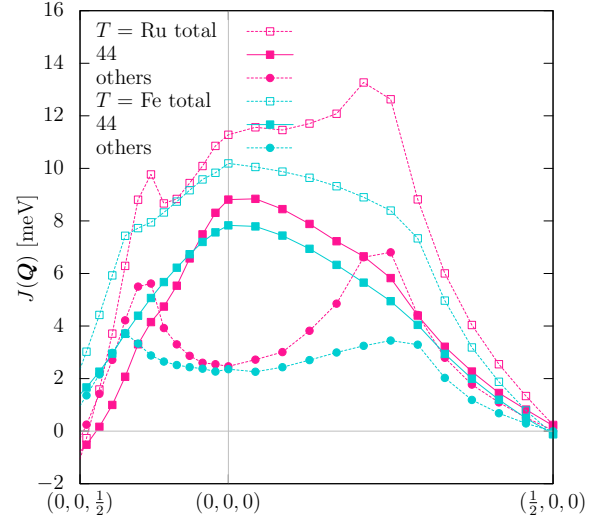


FIG. 7. Orbital decomposed $J(\mathbf{q})$ calculated by the Liechtenstein method. The total (dotted line with open square), diagonal $d_{x^2-y^2}$ orbital (solid line with filled square), and the other contribution (dotted like with filled circle) are shown. The pink and cyan lines correspond to the results for GdRu₂Si₂ and GdFe₂Si₂, respectively.

whether the system favors the ferromagnetic or finite- \mathbf{Q} spin spiral state depends on the competition between the contributions from $d_{x^2-y^2}$ and the other orbitals. Notably, this situation is realized not only in GdRu₂Si₂ but also in GdFe₂Si₂ as is shown in Fig. 7. The figure shows why these two compounds favor different magnetic structures though they share almost the same Fermi surface. Namely, the contribution from the $d_{x^2-y^2}$ orbital relative to that from the other d orbitals is larger in GdFe₂Si₂ than GdRu₂Si₂. This is mainly due to the suppression of the finite- \mathbf{Q} peak in the contribution from the other d orbitals in GdFe₂Si₂.

Here, let us look into the detail of the microscopic origin of $J(\mathbf{q})$ based on the following simple model Hamiltonian $H = H_d + H_f + H_{df}$, where,

$$H_d = t_d \sum_{\langle i,j \rangle \sigma} d_{i\sigma}^\dagger d_{j\sigma} + U_d \sum_i n_{i\uparrow}^d n_{i\downarrow}^d, \quad (11)$$

$$H_f = t_f \sum_{\langle i,j \rangle \sigma} f_{i\sigma}^\dagger f_{j\sigma} + U_f \sum_i n_{i\uparrow}^f n_{i\downarrow}^f, \quad (12)$$

$$H_{df} = V \sum_{i\sigma} (d_{i\sigma}^\dagger f_{i\sigma} + f_{i\sigma}^\dagger d_{i\sigma}) + J_{cf} \sum_i \mathbf{s}^d \cdot \mathbf{s}^f. \quad (13)$$

Here, H_d , H_f and H_{df} represent terms for the Gd-5d orbitals, 4f orbitals and their hybridization terms, respectively. Our calculations for GdT₂X₂ show that, in the presence of U , the 5d contribution always overcomes that of 4f since the latter is strongly suppressed. This clearly indicates that both the super-exchange interaction $J_{\text{ex}}^f \sim t_f^2/U_f$ and the conventional RKKY interaction $J_{\text{RKKY}} \sim (V^2/U_f)^2 \chi^d$, where χ^d is the spin susceptibility in the 5d orbitals, are negligibly small in these

compounds. Conversely, the strong magnetic interaction from the $5d$ orbitals can be easily understood since they have large DOS near the Fermi level, and have a finite exchange splitting due to the magnetic ordering although it is not as large as that of the $4f$ orbitals. Here, we note that there are two possibilities for the origin of the exchange splitting in the $5d$ states. One is the Coulomb interaction inherent in the $5d$ orbitals, *i.e.*, the second term in eq. (11), in which case the spin instability is described purely by the $5d$ orbitals. The other is the magnetic coupling between the $5d$ and $4f$ orbitals, *i.e.*, the second term in eq. (13), which one may call "generalized" RKKY interaction since it comes from the coupling between conduction bands and local spins [66]. It should be noted that in SDFT+ U , the correlation effect is included in the exchange-correlation functional, and the many-body problem turns into an effective one-body calculation. Then, we can not distinguish these two contributions from the resulting exchange splittings. Investigating the microscopic origin of $J(\mathbf{q})$ more precisely requires more elaborated calculations, such as a calculation combined with dynamical mean-field approximation [67]. This direction of development is an interesting and important future task in this field.

E. Systematic evaluation of $J(\mathbf{q})$ based on the Liechtenstein method

Let us move on to the results of $J(\mathbf{q})$ calculated with SDFT+ U for $\text{Gd}T_2X_2$ and $\text{Eu}T_2X_2$ in Fig. 8 and Fig. 9, respectively. From these figures, we see that the general trend of $J(\mathbf{q})$ is not sensitive to the choice of group 14 elements $X = \text{Si}$ or Ge . On the other hand, the choices of different f -elements and different periods (*i.e.*, $3d$, $4d$, or $5d$) of the transition metals T dramatically change the structure of $J(\mathbf{q})$. For example, for the $\text{Gd}T_2X_2$ compounds, the T dependence of group 5 ($T = \text{V}, \text{Nb}, \text{Ta}$), 8 ($T = \text{Fe}, \text{Ru}, \text{Os}$), and 9 ($T = \text{Co}, \text{Rh}, \text{Ir}$) are not so significant. On the other hand, for $\text{Eu}T_2X_2$, the T dependence is more noticeable. These dependencies may come from the chemical pressure effects on the lattice structures or the spreads and local energy levels of the d -orbitals.

According to Figs. 8 and 9, the most promising candidates showing skyrmion lattice phase would be compounds with T being the group 8 transition metal. In particular, GdRu_2Si_2 , GdRu_2Ge_2 , GdOs_2Si_2 , GdOs_2Ge_2 , and EuOs_2Si_2 have the highest peaks at finite \mathbf{Q} along the Γ - X line. Together with the small easy-axis anisotropy shown in Figs. 2(a-d), they should show the skyrmion lattice phase, and indeed, it is already found in GdRu_2Si_2 . Except for these compounds, we can also see that GdW_2X_2 , GdRe_2X_2 , GdAg_2X_2 , GdAu_2X_2 , EuCo_2X_2 , and EuAg_2X_2 with $X = \text{Si}$ and Ge have the highest peaks along the Γ - X line. However, the peaks in GdW_2X_2 and EuCo_2X_2 may be too small to stabilize the magnetic order.

F. Modulation vector based on spin spiral calculations

Up to now, we have discussed the magnetic interaction $J(\mathbf{q})$ and the corresponding modulation vectors \mathbf{Q} based on the Liechtenstein method. The calculations are performed for the Wannier tight-binding models derived from first-principles for the ferromagnetic ground states. Thus, in principle, the reliability of the \mathbf{q} -dependence far from the Γ point, as well as the validity of the mapping to the classical spin model cannot be justified. Here, we present spin spiral calculations for the materials expected to be a good candidate for showing the skyrmion phase. Since the calculation is exact within the SDFT+ U level, the results can be used in a way complementary to that of the Liechtenstein method.

Figure 10(a) shows the \mathbf{q} -dependence of the total energies for $\text{Gd}T_2X_2$ with $T = \text{Fe}, \text{Ru}, \text{Os}$. The calculations are performed by the spin spiral calculations based on SDFT+ U with $U = 6.7$ and $J = 0.7$ eV. Since the minimum position of $E(\mathbf{q})$ represents the most stable modulation vector, we can see that GdRu_2Si_2 , GdRu_2Ge_2 , and GdOs_2Si_2 favor the finite- \mathbf{Q} state with $\mathbf{Q} \sim (0.20, 0, 0)$ -($0.25, 0, 0$). On the other hand, GdFe_2Si_2 and GdFe_2Ge_2 have the minimum at the Γ point, indicating that the ferromagnetic state is the most stable. These features are in good agreement with the calculations based on the Liechtenstein method. Although the GdOs_2Ge_2 does not show the finite- \mathbf{Q} instability in contrast with the Liechtenstein result, the peak of $J(\mathbf{q})$ in GdOs_2Si_2 is more fragile than the others as is shown in Fig. 8(e). Thus, the disagreement with the Liechtenstein method is not serious. For the comparison, we also show $E(\mathbf{q})$ of $\text{Gd}T_2X_2$ with $T = \text{Fe}, \text{Ru}, \text{Os}$ and $X = \text{Si}, \text{Ge}$ based on SDFT in Fig. 10(b). We can see that the finite- \mathbf{Q} instability becomes stronger in all cases than in SDFT+ U . Here, GdFe_2Si_2 shows the finite- \mathbf{Q} instability in SDFT while it does not in SDFT+ U , which again agrees well with the Liechtenstein calculations. In Fig. 10(c), we show $E(\mathbf{q})$ for the other candidates for showing the skyrmion phase predicted by the Liechtenstein calculations, namely, $\text{Gd}T_2X_2$ with $T = \text{Re}, \text{Ag}, \text{Au}$ and $X = \text{Si}, \text{Ge}, \text{EuAg}_2\text{Si}_2$ and EuAg_2Ge_2 . We can see that GdRe_2Si_2 , and GdRe_2Ge_2 show nearly flat \mathbf{q} dependence near the Γ point, and thus, it is possible that some subtle perturbations select a finite- \mathbf{Q} state. On the other hand, GdAg_2X_2 , GdAu_2X_2 , and EuAg_2X_2 have a broad peak at $\mathbf{Q} \sim (\frac{1}{2}, 0, 0)$ corresponding to the 90-degree rotating structure with the nearest neighboring spins, which seems to be too large to realize a skyrmion phase. However, due to its broad nature, we may still have a chance to achieve a skyrmion phase with smaller \mathbf{Q} in experiments by using, for example, chemical substitution and external pressure. We leave the possible magnetic structures favored in these compounds as a future study.

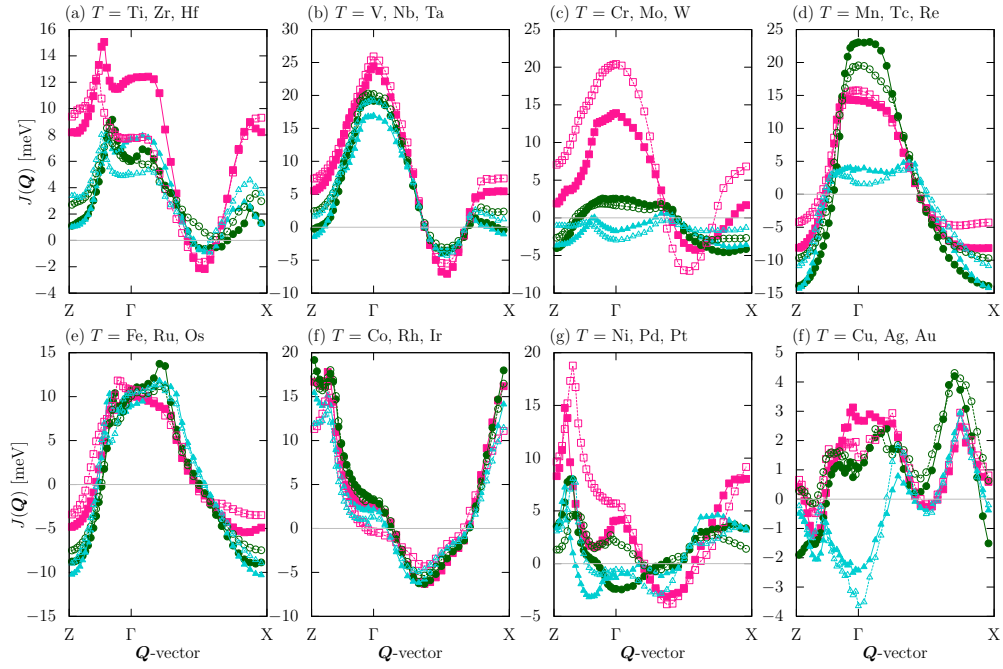


FIG. 8. Spin interactions $J(\mathbf{q})$ in $\text{Gd}T_2X_2$ calculated by the Liechtenstein method based on the SDFT+ U electronic structures. The pink, green, and cyan lines with square, circle, and triangle points correspond to $3d$, $4d$, and $5d$ elements as T , respectively. The solid (dashed) lines with filled (open) symbols stand for $X = \text{Si}$ (Ge). Note that the high symmetry points Z , Γ , and X correspond to $(0, 0, \frac{2\pi}{c})$, $(0, 0, 0)$ and $(\frac{2\pi}{a}, 0, 0)$ in the cartesian frame of the reciprocal lattice space, respectively.

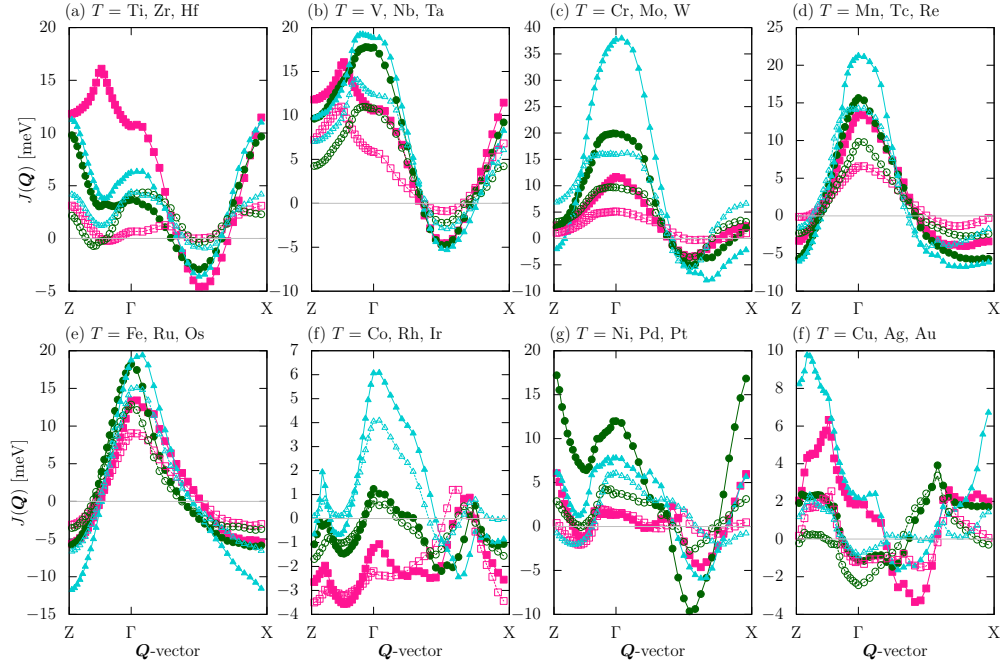


FIG. 9. Spin interactions $J(\mathbf{q})$ in $\text{Eu}T_2X_2$ calculated by the Liechtenstein method based on the SDFT+ U electronic structures. Color, line and point types are the same as Fig. 8.

V. CONCLUSION AND OUTLOOK

In this *Perspective*, we present systematic first-principles calculations for $\text{Gd}T_2X_2$ and $\text{Eu}T_2X_2$ with

T being a transition metal element and X being Si or Ge. From the magnetocrystalline anisotropy calculations based on SDFT and SDFT+ U , we show that the inclusion of Coulomb interaction U and Hund's coupling J

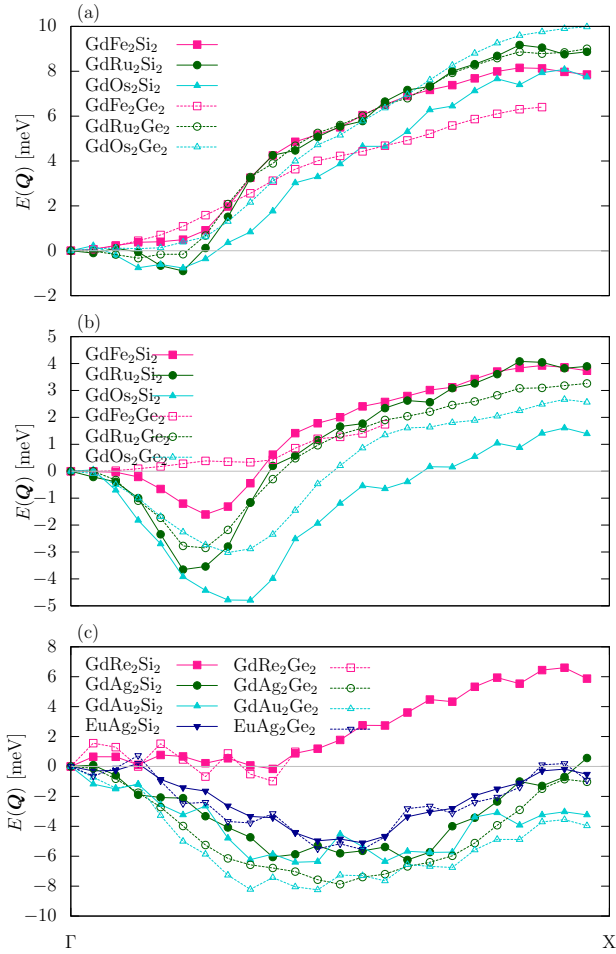


FIG. 10. Modulation vector \mathbf{q} dependence of the ground state energy $E(\mathbf{q})$ calculated based on the Frozen magnon method. (a) The results based on the SDFT+ U with $U = 6.7$ eV and $J = 0.7$ eV for GdT_2X_2 with $T = \text{Fe, Ru, Os}$ and $X = \text{Si, Ge}$. (b) The results based on the SDFT for GdT_2X_2 with $T = \text{Fe, Ru, Os}$ and $X = \text{Si, Ge}$. (c) The results based on the SDFT+ U with $U = 6.7$ eV and $J = 0.7$ eV for GdT_2X_2 with $T = \text{Re, Ag, Au}$ and $X = \text{Si, Ge}$.

is essential to obtain the easy-axis anisotropy. Then, based on the SDFT+ U electronic structures, we evaluate magnetic interactions $J(\mathbf{q})$ based on the Liechtenstein method and show that the obtained $J(\mathbf{q})$ is in good agreement with $E(\mathbf{q})$ by the spin spiral calcula-

tions. Our calculations indicate that the finite- \mathbf{Q} structure is determined not only by the Fermi surface topology but also by the details of the electronic structure, and the competition of each Gd-5d orbital contribution determines whether a ferromagnetic spin configuration or finite- \mathbf{Q} structure is favored in GdT_2Si_2 with $T = \text{Fe}$ and Ru . According to our calculations, GdRu_2X_2 , GdOs_2X_2 , and GdRe_2X_2 are promising candidates, while GdAg_2X_2 , GdAu_2X_2 , and EuAg_2X_2 are possible candidates for showing the skyrmion lattice phase. Since the systematic calculations based on the Liechtenstein method is shown to be helpful in evaluating the finite- \mathbf{Q} structure, the extension to other crystal structure would be a possible direction to discover and engineer new skyrmion compounds. On the other hand, developing new methods to evaluate transport properties in the short pitch skyrmion phase is another crucial direction for its practical applications. Since most of the novel phenomena associated with its high skyrmion density have been studied based on simple models, further development is necessary to achieve a better understanding of material dependence and quantitative evaluations.

VI. ACKNOWLEDGMENTS

This work was supported by JSPS-KAKENHI (No. 22H00290, 21H04437, 21H04990, and 19H05825) and JST-PRESTO (No. JPMJPR20L7). We also acknowledge the Center for Computational Materials Science, Institute for Materials Research, Tohoku University, for the use of MASAMUNE-IMR (Project No. 202112-SCKXX-0010).

VII. AUTHOR DECLARATIONS

Conflict of Interest

The authors have no conflicts to disclose.

Author Contributions

Takuya Nomoto: Formal analysis (lead); Writing - original draft. Ryotaro Arita: Formal analysis (supporting); Writing - review & editing.

DATA AVAILABILITY

The data that support the findings of this study are available from the corresponding author upon reasonable request.

[1] N. Nagaosa and Y. Tokura, Topological properties and dynamics of magnetic skyrmions, *Nature Nanotechnology* **8**, 899 (2013).
 [2] B. Göbel, I. Mertig, and O. A. Tretiakov, Beyond skyrmions: Review and perspectives of alternative magnetic quasiparticles, *Physics Reports* **895**, 1 (2021), beyond skyrmions: Review and perspectives of alternative magnetic quasiparticles.

[3] Y. Tokura and N. Kanazawa, Magnetic skyrmion materials, *Chemical Reviews* **121**, 2857 (2021), PMID: 33164494.
 [4] G. Finocchio, F. B. ttner, R. Tomasello, M. Carpentieri, and M. Kläui, Magnetic skyrmions: from fundamental to applications, *Journal of Physics D: Applied Physics* **49**, 423001 (2016).
 [5] A. Fert, N. Reyren, and V. Cros, Magnetic skyrmions:

- advances in physics and potential applications, *Nature Reviews Materials* **2**, 17031 (2017).
- [6] S. Luo and L. You, Skyrmion devices for memory and logic applications, *APL Materials* **9**, 050901 (2021).
- [7] C. H. Marrows and K. Zeissler, Perspective on skyrmion spintronics, *Applied Physics Letters* **119**, 250502 (2021).
- [8] H. Wang, Y. Dai, G.-M. Chow, and J. Chen, Topological hall transport: Materials, mechanisms and potential applications, *Progress in Materials Science* **130**, 100971 (2022).
- [9] S. S. P. Parkin, M. Hayashi, and L. Thomas, Magnetic domain-wall racetrack memory, *Science* **320**, 190 (2008).
- [10] J. Sampaio, V. Cros, S. Rohart, A. Thiaville, and A. Fert, Nucleation, stability and current-induced motion of isolated magnetic skyrmions in nanostructures, *Nature Nanotechnology* **8**, 839 (2013).
- [11] X. Zhang, W. Cai, X. Zhang, Z. Wang, Z. Li, Y. Zhang, K. Cao, N. Lei, W. Kang, Y. Zhang, H. Yu, Y. Zhou, and W. Zhao, Skyrmions in magnetic tunnel junctions, *ACS Applied Materials & Interfaces* **10**, 16887 (2018).
- [12] Y. Huang, W. Kang, X. Zhang, Y. Zhou, and W. Zhao, Magnetic skyrmion-based synaptic devices, *Nanotechnology* **28**, 08LT02 (2017).
- [13] K. M. Song, J.-S. Jeong, B. Pan, X. Zhang, J. Xia, S. Cha, T.-E. Park, K. Kim, S. Finizio, J. Raabe, J. Chang, Y. Zhou, W. Zhao, W. Kang, H. Ju, and S. Woo, Skyrmion-based artificial synapses for neuromorphic computing, *Nature Electronics* **3**, 148 (2020).
- [14] Y. S. Lin, P. J. Grundy, and E. A. Giess, Bubble domains in magnetostatically coupled garnet films, *Applied Physics Letters* **23**, 485 (1973).
- [15] T. Garel and S. Doniach, Phase transitions with spontaneous modulation-the dipolar ising ferromagnet, *Phys. Rev. B* **26**, 325 (1982).
- [16] S. Mühlbauer, B. Binz, F. Jonietz, C. Pfleiderer, A. Rosch, A. Neubauer, R. Georgii, and P. Böni, Skyrmion lattice in a chiral magnet, *Science* **323**, 915 (2009).
- [17] A. N. Bogdanov and D. A. Yablonskii, Thermodynamically stable “vortices” in magnetically ordered crystals. the mixed state of magnets, *Sov. Phys. JETP* **68**, 101 (1989).
- [18] U. K. Röbller, A. N. Bogdanov, and C. Pfleiderer, Spontaneous skyrmion ground states in magnetic metals, *Nature* **442**, 797 (2006).
- [19] A. Fert and P. M. Levy, Role of anisotropic exchange interactions in determining the properties of spin-glasses, *Phys. Rev. Lett.* **44**, 1538 (1980).
- [20] M. Heide, G. Bihlmayer, and S. Blügel, Dzyaloshinskii-moriya interaction accounting for the orientation of magnetic domains in ultrathin films: Fe/w(110), *Phys. Rev. B* **78**, 140403 (2008).
- [21] F. Freimuth, S. B. gel, and Y. Mokrousov, Berry phase theory of dzyaloshinskii– moriya interaction and spin-orbit torques, *Journal of Physics: Condensed Matter* **26**, 104202 (2014).
- [22] T. Kikuchi, T. Koretsune, R. Arita, and G. Tatara, Dzyaloshinskii-moriya interaction as a consequence of a doppler shift due to spin-orbit-induced intrinsic spin current, *Phys. Rev. Lett.* **116**, 247201 (2016).
- [23] T. Koretsune, T. Kikuchi, and R. Arita, First-principles evaluation of the dzyaloshinskii– moriya interaction, *Journal of the Physical Society of Japan* **87**, 041011 (2018).
- [24] S. R. Saha, H. Sugawara, T. D. Matsuda, H. Sato, R. Mallik, and E. V. Sampathkumaran, Magnetic anisotropy, first-order-like metamagnetic transitions, and large negative magnetoresistance in single-crystal gd_2pdsi_3 , *Phys. Rev. B* **60**, 12162 (1999).
- [25] T. Kurumaji, T. Nakajima, M. Hirschberger, A. Kikkawa, Y. Yamasaki, H. Sagayama, H. Nakao, Y. Taguchi, T. hisa Arima, and Y. Tokura, Skyrmion lattice with a giant topological hall effect in a frustrated triangular-lattice magnet, *Science* **365**, 914 (2019).
- [26] M. Hirschberger, T. Nakajima, S. Gao, L. Peng, A. Kikkawa, T. Kurumaji, M. Kriener, Y. Yamasaki, H. Sagayama, H. Nakao, K. Ohishi, K. Kakurai, Y. Taguchi, X. Yu, T.-h. Arima, and Y. Tokura, Skyrmion phase and competing magnetic orders on a breathing kagomé lattice, *Nature Communications* **10**, 5831 (2019).
- [27] N. D. Khanh, T. Nakajima, X. Yu, S. Gao, K. Shibata, M. Hirschberger, Y. Yamasaki, H. Sagayama, H. Nakao, L. Peng, K. Nakajima, R. Takagi, T.-h. Arima, Y. Tokura, and S. Seki, Nanometric square skyrmion lattice in a centrosymmetric tetragonal magnet, *Nature Nanotechnology* **15**, 444 (2020).
- [28] T. Shang, Y. Xu, D. J. Gawryluk, J. Z. Ma, T. Shiroka, M. Shi, and E. Pomjakushina, Anomalous hall resistivity and possible topological hall effect in the eua_4 antiferromagnet, *Phys. Rev. B* **103**, L020405 (2021).
- [29] K. Kaneko, T. Kawasaki, A. Nakamura, K. Munakata, A. Nakao, T. Hanashima, R. Kiyonagi, T. Ohhara, M. Hedo, T. Nakama, and Y. Ōnuki, Charge-density-wave order and multiple magnetic transitions in divalent europium compound eua_4 , *Journal of the Physical Society of Japan* **90**, 064704 (2021).
- [30] X. Y. Zhu, H. Zhang, D. J. Gawryluk, Z. X. Zhen, B. C. Yu, S. L. Ju, W. Xie, D. M. Jiang, W. J. Cheng, Y. Xu, M. Shi, E. Pomjakushina, Q. F. Zhan, T. Shiroka, and T. Shang, Spin order and fluctuations in the eua_4 and euga_4 topological antiferromagnets: A μSR study, *Phys. Rev. B* **105**, 014423 (2022).
- [31] R. Takagi, N. Matsuyama, V. Ukleev, L. Yu, J. S. White, S. Francoual, J. R. L. Mardegan, S. Hayami, H. Saito, K. Kaneko, K. Ohishi, Y. Ōnuki, T.-h. Arima, Y. Tokura, T. Nakajima, and S. Seki, Square and rhombic lattices of magnetic skyrmions in a centrosymmetric binary compound, *Nature Communications* **13**, 1472 (2022).
- [32] H. Zhang, X. Y. Zhu, Y. Xu, D. J. Gawryluk, W. Xie, S. L. Ju, M. Shi, T. Shiroka, Q. F. Zhan, E. Pomjakushina, and T. Shang, Giant magnetoresistance and topological hall effect in the euga_4 antiferromagnet, *Journal of Physics: Condensed Matter* **34**, 034005 (2021).
- [33] Y. Ōnuki, M. Kakihana, W. Iha, K. Nakaima, D. Aoki, A. Nakamura, F. Honda, M. Nakashima, Y. Amako, J. Gouchi, Y. Uwatoko, S. Nakamura, T. Sakakibara, T. Takeuchi, Y. Haga, H. Ikeda, H. Harima, M. Hedo, and T. Nakama, Unique skyrmion phases and conduction electrons in cubic chiral antiferromagnet euPtSi and related compounds, in *Proceedings of the International Conference on Strongly Correlated Electron Systems (SCES2019)*.
- [34] T. Sakakibara, S. Nakamura, S. Kittaka, M. Kakihana, M. Hedo, T. Nakama, and Y. Ōnuki, Magnetic phase transitions of the 4f skyrmion compound euPtSi studied by magnetization measurements, *Journal of the Physical Society of Japan* **90**, 064701 (2021).

- [35] N. Kanazawa, Y. Onose, T. Arima, D. Okuyama, K. Ohoyama, S. Wakimoto, K. Kakurai, S. Ishiwata, and Y. Tokura, Large topological hall effect in a short-period helimagnet mngge, *Phys. Rev. Lett.* **106**, 156603 (2011).
- [36] K. Shibata, X. Z. Yu, T. Hara, D. Morikawa, N. Kanazawa, K. Kimoto, S. Ishiwata, Y. Matsui, and Y. Tokura, Towards control of the size and helicity of skyrmions in helimagnetic alloys by spin-orbit coupling, *Nature Nanotechnology* **8**, 723 (2013).
- [37] K. Hamamoto, M. Ezawa, and N. Nagaosa, Quantized topological hall effect in skyrmion crystal, *Phys. Rev. B* **92**, 115417 (2015).
- [38] A. Matsui, T. Nomoto, and R. Arita, Skyrmion-size dependence of the topological hall effect: A real-space calculation, *Phys. Rev. B* **104**, 174432 (2021).
- [39] T. Okubo, S. Chung, and H. Kawamura, Multiple- q states and the skyrmion lattice of the triangular-lattice heisenberg antiferromagnet under magnetic fields, *Phys. Rev. Lett.* **108**, 017206 (2012).
- [40] A. O. Leonov and M. Mostovoy, Multiply periodic states and isolated skyrmions in an anisotropic frustrated magnet, *Nature Communications* **6**, 8275 (2015).
- [41] J. P. Chen, D.-W. Zhang, and J.-M. Liu, Exotic skyrmion crystals in chiral magnets with compass anisotropy, *Scientific Reports* **6**, 29126 (2016).
- [42] J. Chen, D.-W. Zhang, Y. Chen, X. Gao, and J.-M. Liu, Compass-anisotropy-modulated helical states and skyrmion crystals in chiral magnets, *Physics Letters A* **382**, 2944 (2018).
- [43] S. Heinze, K. von Bergmann, M. Menzel, J. Brede, A. Kubetzka, R. Wiesendanger, G. Bihlmayer, and S. Blügel, Spontaneous atomic-scale magnetic skyrmion lattice in two dimensions, *Nature Physics* **7**, 713 (2011).
- [44] S. Hayami, R. Ozawa, and Y. Motome, Effective bilinear-biquadratic model for noncoplanar ordering in itinerant magnets, *Phys. Rev. B* **95**, 224424 (2017).
- [45] R. Ozawa, S. Hayami, K. Barros, G.-W. Chern, Y. Motome, and C. D. Batista, Vortex crystals with chiral stripes in itinerant magnets, *Journal of the Physical Society of Japan* **85**, 103703 (2016).
- [46] R. Ozawa, S. Hayami, and Y. Motome, Zero-field skyrmions with a high topological number in itinerant magnets, *Phys. Rev. Lett.* **118**, 147205 (2017).
- [47] S. Hayami and Y. Motome, Topological spin crystals by itinerant frustration, *Journal of Physics: Condensed Matter* **33**, 443001 (2021).
- [48] T. Nomoto, T. Koretsune, and R. Arita, Formation mechanism of the helical q structure in gd-based skyrmion materials, *Phys. Rev. Lett.* **125**, 117204 (2020).
- [49] J. Bouaziz, E. Mendive-Tapia, S. Blügel, and J. B. Staunton, Fermi-surface origin of skyrmion lattices in centrosymmetric rare-earth intermetallics, *Phys. Rev. Lett.* **128**, 157206 (2022).
- [50] S. Grytsiuk, J.-P. Hanke, M. Hoffmann, J. Bouaziz, O. Gomonay, G. Bihlmayer, S. Lounis, Y. Mokrousov, and S. Blügel, Topological-chiral magnetic interactions driven by emergent orbital magnetism, *Nature Communications* **11**, 511 (2020).
- [51] E. Mendive-Tapia, M. dos Santos Dias, S. Grytsiuk, J. B. Staunton, S. Blügel, and S. Lounis, Short period magnetization texture of b20-mngge explained by thermally fluctuating local moments, *Phys. Rev. B* **103**, 024410 (2021).
- [52] D. M. Korotin, V. V. Mazurenko, V. I. Anisimov, and S. V. Streltsov, Calculation of exchange constants of the heisenberg model in plane-wave-based methods using the green's function approach, *Phys. Rev. B* **91**, 224405 (2015).
- [53] T. Nomoto, T. Koretsune, and R. Arita, Local force method for the ab initio tight-binding model: Effect of spin-dependent hopping on exchange interactions, *Phys. Rev. B* **102**, 014444 (2020).
- [54] A. A. Mostofi, J. R. Yates, Y.-S. Lee, I. Souza, D. Vanderbilt, and N. Marzari, wannier90: A tool for obtaining maximally-localised wannier functions, *Computer Physics Communications* **178**, 685 (2008).
- [55] N. Marzari, A. A. Mostofi, J. R. Yates, I. Souza, and D. Vanderbilt, Maximally localized wannier functions: Theory and applications, *Rev. Mod. Phys.* **84**, 1419 (2012).
- [56] N. Chikano, K. Yoshimi, J. Otsuki, and H. Shinaoka, irbasis: Open-source database and software for intermediate-representation basis functions of imaginary-time green's function, *Computer Physics Communications* **240**, 181 (2019).
- [57] J. Li, M. Wallerberger, N. Chikano, C.-N. Yeh, E. Gull, and H. Shinaoka, Sparse sampling approach to efficient ab initio calculations at finite temperature, *Phys. Rev. B* **101**, 035144 (2020).
- [58] L. M. Sandratskii, Noncollinear magnetism in itinerant-electron systems: Theory and applications, *Advances in Physics* **47**, 91 (1998).
- [59] G. Kresse and J. Furthmüller, Efficient iterative schemes for ab initio total-energy calculations using a plane-wave basis set, *Phys. Rev. B* **54**, 11169 (1996).
- [60] J. P. Perdew, K. Burke, and M. Ernzerhof, Generalized gradient approximation made simple, *Phys. Rev. Lett.* **77**, 3865 (1996).
- [61] P. E. Blöchl, Projector augmented-wave method, *Phys. Rev. B* **50**, 17953 (1994).
- [62] G. Kresse and D. Joubert, From ultrasoft pseudopotentials to the projector augmented-wave method, *Phys. Rev. B* **59**, 1758 (1999).
- [63] A. Garnier, D. Gignoux, N. Iwata, D. Schmitt, T. Shigeoka, and F. Zhang, Anisotropic metamagnetism in gdru2si2, *Journal of Magnetism and Magnetic Materials* **140-144**, 899 (1995), international Conference on Magnetism.
- [64] M. Mihalik, P. Svoboda, M. Mihalik, J. Vejpravová, and V. Sechovský, Magnetic and transport properties of gdfe2si2 single-crystal, *Journal of Magnetism and Magnetic Materials* **290-291**, 606 (2005), proceedings of the Joint European Magnetic Symposia (JEMS' 04).
- [65] Y. O. Kvashnin, R. Cardias, A. Szilva, I. Di Marco, M. I. Katsnelson, A. I. Lichtenstein, L. Nordström, A. B. Klautau, and O. Eriksson, Microscopic origin of heisenberg and non-heisenberg exchange interactions in ferromagnetic bcc fe, *Phys. Rev. Lett.* **116**, 217202 (2016).
- [66] J. Bouaziz and S. Blügel, in private communication.
- [67] M. I. Katsnelson and A. I. Lichtenstein, First-principles calculations of magnetic interactions in correlated systems, *Phys. Rev. B* **61**, 8906 (2000).